

---

# Fully Transformer Networks for Semantic Image Segmentation

---

Sitong Wu<sup>1,2\*</sup>, Tianyi Wu<sup>1,2\*</sup>, Fangjian Lin<sup>1,2,3\*</sup>, Shengwei Tian<sup>3</sup>, Guodong Guo<sup>1,2†</sup>

<sup>1</sup>Institute of Deep Learning, Baidu Research, Beijing, China

<sup>2</sup>National Engineering Laboratory for Deep Learning Technology and Application, Beijing, China

<sup>3</sup>School of Software, XinJiang University, urumqi, China

{v\_wusitong, wutianyi01, v\_linfangjian, guogudong01}@baidu.com, tianshengwei@163.com

## Abstract

Transformers have shown impressive performance in various natural language processing and computer vision tasks, due to the capability of modeling long-range dependencies. Recent progress has demonstrated that combining such transformers with CNN-based semantic image segmentation models is very promising. However, it is not well studied yet on how well a pure transformer based approach can achieve for image segmentation. In this work, we explore a novel framework for semantic image segmentation, which is encoder-decoder based Fully Transformer Networks (FTN). Specifically, we first propose a Pyramid Group Transformer (PGT) as the encoder for progressively learning hierarchical features, while reducing the computation complexity of the standard visual transformer(ViT). Then, we propose a Feature Pyramid Transformer (FPT) to fuse semantic-level and spatial-level information from multiple levels of the PGT encoder for semantic image segmentation. Surprisingly, this simple baseline can achieve new state-of-the-art results on multiple challenging semantic segmentation benchmarks, including PASCAL Context, ADE20K and COCO-Stuff. The source code will be released upon the publication of this work.

## 1 Introduction

Semantic image segmentation aims to assign a semantic label to each pixel in an image, which is an indispensable component for many applications, such as autonomous vehicles [11], human-computer interaction [18], and medical diagnosis [16]. Since the era of deep learning, convolutional neural networks (CNNs) have been the cornerstone of tremendous image segmentation models.

Inspired by successful applications of transformers on natural language processing tasks (machine translation [33], text classification [20]), and computer vision tasks (image classification [13, 44, 46, 48, 29, 57, 26]), Transformer has attracted more and more interests in the context of semantic image segmentation [60, 38, 46, 29, 51] recently. These methods combined the transformer module into the encoder-decoder architecture, where the encoder reduces the feature maps and captures rich semantic representations, while the decoder gradually recovers the spatial information or fuses multi-scale representation for generating accurate pixel-level predictions. These approaches can be divided into three categories: (1) **Transformer-CNN architecture** [38, 46, 60, 29]. It contains a transformer encoder and CNN decoder. Images are first divided into a set of patches and projected to patch embeddings, which are then passed through a transformer encoder and a traditional CNN decoder to recover the pixel-level prediction, as shown in Figure 1(a). (2) **Hybrid-CNN architecture** [60]. As

---

\* Equal contribution.

† Corresponding author.

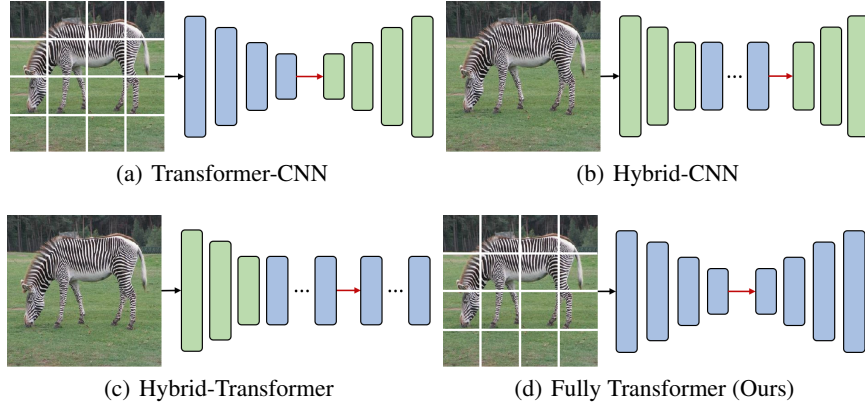


Figure 1: Pipelines of the previous Transformer-based segmentation models. The blue bar represents Transformer blocks and the green bar indicates CNN layers. The encoder and decoder are separated by a red snip.

shown in Figure 1(b), its decoder is the traditional CNN, while the encoder is a combination of CNN (e.g., ResNet, or ResNeXt) and transformer layers, the output of CNN with a lower resolution is directly used as the patch embeddings for transformer layers. (3) **Hybrid-Transformer architecture** [51]. It further replaced the CNN decoder with transformer decoder compared to the Hybrid-CNN, as shown in Figure 1(c).

Different from the methods mentioned above, we propose Fully Transformer Networks (FTN) for semantic image segmentation, without relying on CNN. As shown in Figure 1(d), both the encoder and decoder in the proposed FTN are composed of multiple transformer modules. Specifically, we first propose a Pyramid Group Transformer (PGT), which divides feature maps into multiple spatial groups, and computes the representation on each spatial group. This endows our model with the capability to handle spatial details or local structures that are designed as an important inductive bias of CNN [55, 58]. Furthermore, PGT reduces the unaffordable computational and memory costs of the standard visual transformer (ViT), which is essential for pixel-level label prediction. Besides, PGT introduces a principle of pyramid structure to reduce the feature resolution and increase the receptive field for extracting hierarchical features. Secondly, we propose a Feature Pyramid Transformer (FPT) decoder to fuse semantic-level and spatial-level information from multiple levels of the PGT encoder, which is essential for image segmentation.

Based on the proposed encoder and decoder, we develop Fully Transformer Networks (FTN) for semantic image segmentation, and evaluated the effectiveness of our approach by conducting extensive ablation studies. Furthermore, we evaluate our FTN on three challenging semantic segmentation benchmarks, including PASCAL-Context [34], ADE20K [61] and COCO-Stuff [4], achieving the state-of-the-art performance (mIoU) of 58.52%, 53.64%, and 48.48%, respectively.

Our main contributions include:

- We propose the Pyramid Group Transformer (PGT) to learn hierarchical representations, while reducing the computation complexity of the standard visual transformer.
- We develop a Feature Pyramid Transformer (FPT) decoder to fuse semantic-level and spatial-level information from multiple levels of the PGT encoder.
- Based on the proposed PGT and FPT, we create Fully Transformer Networks (FTN) for semantic image segmentation, which achieves new state-of-the-art results on multiple challenging benchmarks, including PASCAL Context, ADE20K, and COCO-Stuff.

## 2 Related works

**Semantic Image Segmentation.** The early FCN [30] proposed to use a fully convolutional network to generate predictions for images with an arbitrary size, which is regarded as a milestone in semantic segmentation. For more precise segmentation, some works [35, 2] were devoted to involving fine-

grained details via various hierarchies of decoders. Considering that the effective receptive field of CNN architecture is proved to be much smaller than its theoretical value [32], some works [24, 43] focused on how to integrate global context information for a better scene understanding, which refined the belief maps produced by the unary CNN model through capturing interactions between pixels based on appearance and position similarity. DeepLab family [6, 7, 8] replaced partial pooling layers with atrous convolution to expand the receptive field without reducing the resolution. Besides, PSPNet [59] proposed a general pyramid pooling module to fuse features under four different pyramid scales.

**Self-attention in Semantic Image Segmentation.** Inspired by the success of Transformer [45] for NLP tasks, DANet [15] employed the self-attention [47] on the CNN-based backbone, which adaptively integrated local features with their global dependencies. The traditional self-attention serves as a particularly useful technique for semantic segmentation while being criticized for its prohibitive computation burdens and memory usages. To address this issue, the work [22] and [62] introduced a criss-cross attention mechanism and pyramid sampling module into the self-attention, respectively, aiming to reduce the computation cost and memory usage while keeping the performance. AANet [3] proposed an attention-augmented convolution architecture by concatenating convolutional feature maps with a set of feature maps produced via self-attention. In contrast to these methods which augmented a CNN-based encoder with a self-attention module for semantic segmentation, we propose the novel Fully Transformer Networks, where both encoder and decoder are based on pure Transformer with our specialized design.

**Transformer in Vision Tasks.** DETR [5] combined a common CNN with Transformer for predicting objects, which formulates object detection as a dictionary lookup problem with learnable queries. Later, many researchers explored to adopt a pure transformer architecture for image classification [13, 44, 46, 29, 48, 26, 57, 14]. Vision Transformer (ViT) [13] is the first work to introduce a pure transformer for image classification by treating an image as a sequence of patches. Recently, transformer has attracted more and more attention in semantic segmentation [60, 51, 38]. SETR [60] attempted to introduce transformer for semantic segmentation by using ViT as the encoder and employing CNN-based decoders for generating segmentation results. Trans2Seg [51] stacked a convolution-free encoder-decoder network on the top of a common CNN encoder for transparent object segmentation. DPT [38] assembled tokens from multiple stages of the vision transformer and progressively combined them into full-resolution predictions using a convolutional decoder. Different from these approaches that used transformer as an encoder or decoder, we proposed the encoder-decoder based Fully Transformer Networks for semantic segmentation.

### 3 Method

In this section, we first describe our framework, called Fully Transformer Networks (FTN). Then, we present the encoder architecture of FTN, *i.e.*, Pyramid Group Transformer(PGT), which aims to extract hierarchical representations. Finally, we present the decoder architecture of FTN, *i.e.*, Feature Pyramid Transformer (FPT), which fuses the multi-scale features from the encoder and generates the fine pixel-level label prediction.

#### 3.1 Framework of FTN

The overall framework of our FTN is shown in Figure 2, which consists of Pyramid Group Transformer (PGT) encoder and Feature Pyramid Transformer (FPT) decoder. PGT aims to extract hierarchical representations. It is configured with four stages for learning hierarchical features, similar to some classic backbones [19, 52]. Each stage of PGT has a similar structure, which contains a patch transform layer and multiple PGT blocks. The patch transform layer is employed to reduce the number of tokens. In particular, given an input image  $x \in \mathbb{R}^{H \times W \times 3}$ , it is first transformed into  $\frac{HW}{4^2}$  patches with dimension  $C$  by the patch transform layer in stage 1, then the output is fed into  $N_1$  PGT blocks, where  $N_1$  indicates the number of PGT blocks in stage 1. The output of the last block in stage 1 is  $F_1 \in \mathbb{R}^{\frac{HW}{4^2} \times C}$ . For the last 3 stages, the patch transform layer merges each  $2 \times 2$  non-overlapping neighboring patches to reduce the resolution by 1/2 and expand the dimension twice. The output feature in stage  $i$  is  $F_i \in \mathbb{R}^{\frac{HW}{2^{2i+2}} \times 2^{i-1}C}$ . After getting multi-scale features, we employ FPT decoder to fuse semantic-level and spatial-level information from multiple levels. Finally, the

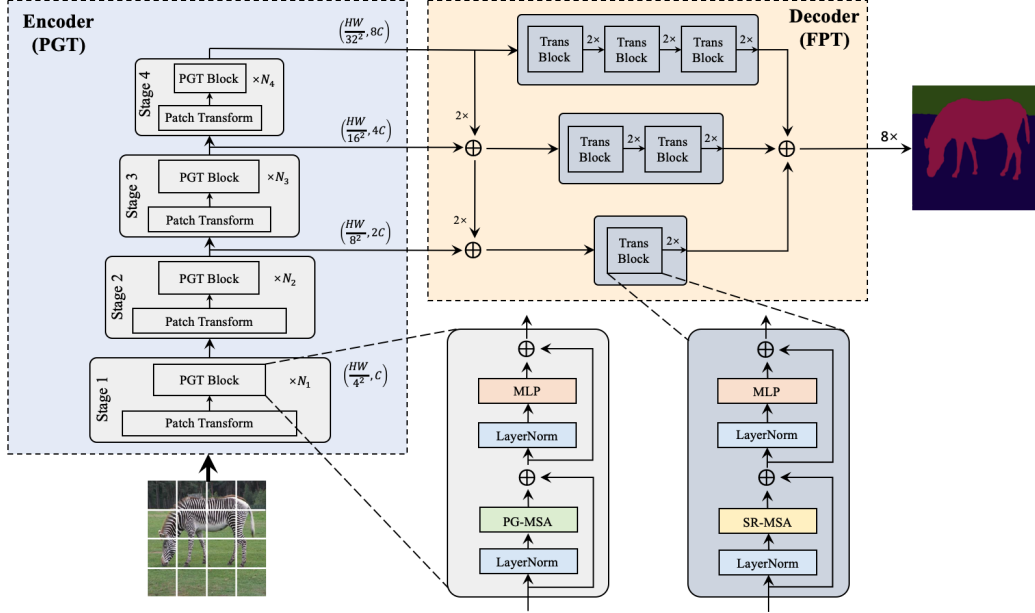


Figure 2: Overall architecture of our Fully Transformer Networks (FTN).

output of FPT is fed into a linear layer followed by a simple bilinear upsampling to generate the probability map for each pixel. The pixel-level segmentation result is obtained by argmax operation on the probability map.

### 3.2 Pyramid Group Transformer

As shown in Figure 2, PGT has four hierarchical stages that generate features with multiple scales. At the beginning of each stage, the features are first shrunk spatially and enlarged in channel dimension by the patch transform layer, and then be fed into the subsequent PGT blocks to learning discriminative representations. PGT progressively increases the receptive field of self-attention when the stage increases, so as to learn low-level spatial details at shallow layers and high-level semantic features at deep layers. Such a mechanism is superior to the previous Vision Transformer (ViT) [13] where the self-attention with a global receptive field is performed on the whole input features at all layers. Besides, our approach can reduce the computational and memory cost of the whole transformer block, which is desired especially for dense prediction tasks.

Specifically, each feature map is firstly divided into non-overlapping grids and each grid is regarded as a group. Then, self-attention is performed among patches within each group. Thus, patches in one group is unacceptable for patches in other groups, which is equivalent to local receptive fields. Explicitly, the size of each receptive field can be conveniently controlled by the group numbers. As shown in Figure 3, the receptive fields at different stages present a pyramid pattern, and we set a consistent receptive field inside each stage. It is notable that the global receptive field is better to be applied in both stage 3 and 4 for the reason that features with stride 16 and 32, usually contain rich semantics. For the  $l$ -th PGT block, its computation can be formulated as follows:

$$\begin{aligned}\hat{Z}^l &= Z^{l-1} + PG\text{-}MSA(LN(Z^{l-1})), \\ Z^l &= \hat{Z}^l + MLP(LN(\hat{Z}^l)),\end{aligned}\tag{1}$$

where  $Z^{l-1}$  is the output of the  $(l-1)$ -th PGT block. LN and MLP refer to layer normalization [1] and multi-layer perceptron, respectively. Furthermore, the core of PGT blocks is the Pyramid Group Multi-Self Attention (PG-MSA), which can be formulated as follow:

$$\begin{aligned}PG\text{-}MSA(Z) &= Concat(h_0, h_1, h_{H-1}), \\ h_i &= Reshape(head_i^0, head_i^1, \dots, head_i^{G-1}), \\ head_i^j &= Attention(Q_i[j], K_i[j], V_i[j]),\end{aligned}\tag{2}$$

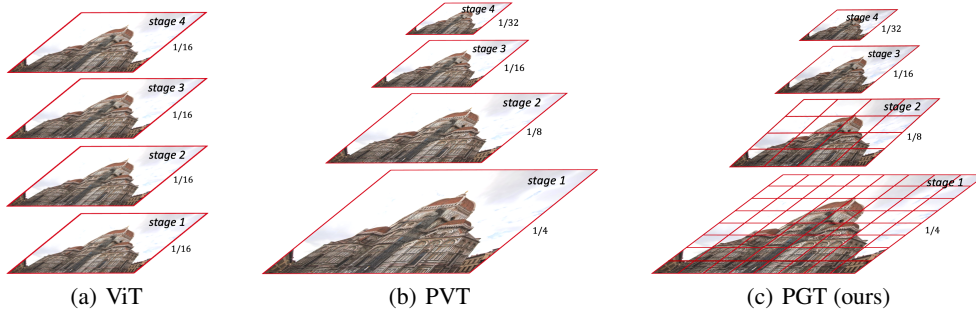


Figure 3: Comparisons of different self-attention mechanisms in Transformers. (a) ViT performed the global self-attention within the single-scale feature maps throughout the whole network. (b) PVT introduced the pyramid structure to generate multi-scale feature maps and applied the global self-attention to features as well. (c) In PGT, the feature map is first divided into groups in spatial domain and then the global self-attention is only performed within each group, i.e., a red grid in the figure. The receptive fields (group size) of attention are progressively increased in stages as a pyramid pattern.

where  $i \in \{0, 1, \dots, H - 1\}$  is the head index;  $j \in \{0, 1, \dots, G - 1\}$  is the group index;  $Attention(\cdot)$  is the self-attention operation [45].  $Q_i = ZW_i^q$ ,  $K_i = ZW_i^k$ , and  $V_i = ZW_i^v$  indicate the query, key, value embedding of the  $i$ -th head, respectively.

**PGT Variants.** We designed 4 variants with different sizes, named PGT-T, PGT-S, PGT-B and PGT-L respectively. For a fair comparison, the sizes of these variants are similar to the previous works [46, 29, 44]. The detailed configuration of our PGT variants are shown in Table 1, where the definitions of hyper-parameters are listed below:

- $P_i^2$ : the token number reduction factor of the patch transform layer in stage  $i$ ;
- $C_i$ : the dimension of tokens in stage  $i$ ;
- $N_i$ : the number of PGT blocks in stage  $i$ ;
- $G_i$ : the group number of PG-MSA in stage  $i$ ;
- $H_i$ : the head number of PG-MSA in stage  $i$ ;
- $E_i$ : the dimension expansion ratio of MLP in stage  $i$ ;

Comparing to the differences among these variants, the representation capacity is only enlarged by increasing the depth of PGT blocks and the dimension of patch tokens (i.e. deeper and wider). For example, PGT-S is obtained by increasing the dimensions of PGT-T, and PGT-B is a deeper version of PGT-S. PGT-L is the deepest and widest among these all. For all variants, the expansion ratio of MLP is set to 4, and the dimension of each head is 32. The pyramid structure of receptive field in attention is also consistent for different variants, with group numbers 64, 16, 1 and 1, respectively, in four stages.

### 3.3 Feature Pyramid Transformer

To generate finer semantic image segmentation, we propose a Feature Pyramid Transformer (FPT) to aggregate the information from multiple levels of the PGT encoder, as shown in Figure 2. Inspired by the spirit of convolution-based FPN [27], FPT is expected to fuse the semantic-level representations and spatial-level information into a high-resolution and high-level semantic output. It follows two simple principles. (1) the top-down connection first hallucinates higher resolution features by upsampling semantically stronger features, and then aggregates these features and spatially finer features whose activations are more accurately localized as it was subsampled fewer times; (2) each level feature is progressively upsampled by the spatial reduction transformer block [46] and bilinear upsampling until it reaches 1/4 scale, and then these multi-level and high-resolution representations are further fused by simple element-wise summation. These two principles enable our model to enhance the capability of fusing multi-level semantic features with different resolutions, which is essential for dense prediction tasks.

Table 1: Detailed configuration of PGT variants.

	Output Stride	Layer Name	PGT-T	PGT-S	PGT-B	PGT-L
Stage 1	4	Patch Transform	$P_1 = 4$			
		PGT Block	$\begin{bmatrix} D_1 = 64 \\ G_1 = 64 \\ H_1 = 2 \\ E_1 = 4 \end{bmatrix} \times 2$	$\begin{bmatrix} D_1 = 96 \\ G_1 = 64 \\ H_1 = 3 \\ E_1 = 4 \end{bmatrix} \times 2$	$\begin{bmatrix} D_1 = 96 \\ G_1 = 64 \\ H_1 = 3 \\ E_1 = 4 \end{bmatrix} \times 2$	$\begin{bmatrix} D_1 = 128 \\ G_1 = 64 \\ H_1 = 4 \\ E_1 = 4 \end{bmatrix} \times 2$
Stage 2	8	Patch Transform	$P_2 = 2$			
		PGT Block	$\begin{bmatrix} D_2 = 128 \\ G_2 = 64 \\ H_2 = 4 \\ E_2 = 4 \end{bmatrix} \times 2$	$\begin{bmatrix} D_2 = 192 \\ G_2 = 64 \\ H_2 = 6 \\ E_2 = 4 \end{bmatrix} \times 2$	$\begin{bmatrix} D_2 = 192 \\ G_2 = 64 \\ H_2 = 6 \\ E_2 = 4 \end{bmatrix} \times 2$	$\begin{bmatrix} D_2 = 256 \\ G_2 = 64 \\ H_2 = 8 \\ E_2 = 4 \end{bmatrix} \times 2$
Stage 3	16	Patch Transform	$P_3 = 2$			
		PGT Block	$\begin{bmatrix} D_3 = 256 \\ G_3 = 64 \\ H_3 = 8 \\ E_3 = 4 \end{bmatrix} \times 6$	$\begin{bmatrix} D_3 = 384 \\ G_3 = 64 \\ H_3 = 12 \\ E_3 = 4 \end{bmatrix} \times 6$	$\begin{bmatrix} D_3 = 384 \\ G_3 = 64 \\ H_3 = 12 \\ E_3 = 4 \end{bmatrix} \times 18$	$\begin{bmatrix} D_3 = 512 \\ G_3 = 64 \\ H_3 = 16 \\ E_3 = 4 \end{bmatrix} \times 18$
Stage 4	32	Patch Transform	$P_4 = 2$			
		PGT Block	$\begin{bmatrix} D_4 = 512 \\ G_4 = 64 \\ H_4 = 16 \\ E_4 = 4 \end{bmatrix} \times 2$	$\begin{bmatrix} D_4 = 768 \\ G_4 = 64 \\ H_4 = 24 \\ E_4 = 4 \end{bmatrix} \times 2$	$\begin{bmatrix} D_4 = 768 \\ G_4 = 64 \\ H_4 = 24 \\ E_4 = 4 \end{bmatrix} \times 2$	$\begin{bmatrix} D_4 = 1024 \\ G_4 = 64 \\ H_4 = 32 \\ E_4 = 4 \end{bmatrix} \times 2$

## 4 Experiments

In this section, we first compare our PGT with the state-of-the-art methods on the image classification task. To further demonstrate the effectiveness of our FTN, we conduct experiments on three widely-used segmentation benchmarks, PASCAL Context [34], ADE20K [61] and COCO-Stuff [4]. Detailed ablation studies are also provided to understand the importance and impact of individual components and settings in our method.

### 4.1 Image Classification

In order to train our FTN on semantic image segmentation benchmarks, we first pretrained our PGT on the ImageNet dataset [39] for obtaining pretrained weights. ImageNet dataset contains 1.3 million images with 1,000 classes. It is referred as ImageNet-1K in this work.

**Experiment Settings.** All the variants are trained for 300 epochs on 8 V100 GPUs from scratch, with a total batch size of 512. We use AdamW [31] as the optimizer with an initial learning rate of 0.0005, cosine decay scheduler, weight decay 0.05, and 5-epoch linear warmup. For data augmentation, we follow most of the widely used settings: random horizontal flipping [40], color jitter, Mixup [56] and AutoAugment [12] and randomly cropping to  $224 \times 224$ . We also use some regularization strategies in [44], such as Label-Smoothing [41] and stochastic depth [21], but without the EMA [36]. During the evaluation, the input image is resized and center-cropped to the size of  $224 \times 224$ . The top-1 accuracy is reported for comparisons.

**Results on ImageNet-1K.** Table 2 shows the comparison with the state-of-the-art CNN and Transformer backbones. Compare to the dominant CNNs, our PGT consistently performs better than the state-of-the-art RegNet [37] and conventional ResNet [19] with similar complexity by a large margin. For example, our PGT-S is +2% higher than RegNet-4G and +3.5% higher than ResNet-50. The advantage of PGT is especially obvious on tiny models, with PGT-T +4.8% higher than PVT-Tiny. For small variants, our PGT-S surpasses the nearest CvT-13 and Swin-T by +0.4% and +0.7%, respectively. Comparing with larger models, our PGT-B and PGT-L exceed PVT significantly by 1~2%, and outperform the state-of-the-art Swin Transformer with similar numbers of parameters and computation budgets, *i.e.*, 83.6 vs. 83.3 and 83.4 vs. 83.0.

Table 2: Comparisons of different backbones for the ImageNet-1K classification. Our PGT consistently outperforms other models with similar numbers of parameters and computation budgets. All experiments are evaluated on the ImageNet validation set with the input size of  $224 \times 224$ .

Method	Image size	Params	GFLOPs	Top-1 Acc. (%)
ResNet-18 [19]	224	12M	1.8	68.5
PVT-Tiny [46]	224	13M	1.9	75.1
ResNet-50 [19]	224	26M	4.1	78.5
DeiT-Small [44]	224	22M	4.6	79.8
PVT-Small [46]	224	25M	3.8	79.8
RegNetY-4G [37]	224	21M	4.0	80.0
T2T-ViT <sub>t</sub> -14 [53]	224	22M	6.1	80.7
TNT-S [17]	224	24M	5.2	81.3
Swin-T [29]	224	29M	4.5	81.3
CvT-13 [48]	224	20M	4.5	81.6
ResNet-101 [19]	224	45M	7.9	79.8
PVT-Medium [46]	224	44M	6.7	81.2
T2T-ViT <sub>t</sub> -19 [53]	224	39M	9.8	81.4
RegNetY-8G [37]	224	39M	8.0	81.7
CvT-21 [48]	224	32M	7.1	82.5
Swin-S [29]	224	50M	8.7	83.0
PVT-Large [46]	224	61M	9.8	81.7
DeiT-Base [44]	224	86M	17.5	81.8
T2T-ViT <sub>t</sub> -24 [53]	224	64M	15.0	82.2
TNT-B [17]	224	66M	14.1	82.8
RegNetY-16G [37]	224	84M	16.0	82.9
Swin-B [29]	224	88M	15.4	83.3
ViT-B/16 [13]	384	86M	55.4	77.9
ViT-L/16 [13]	384	307M	190.7	76.5
PGT-T (ours)	224	13M	2.1	79.9
PGT-S (ours)	224	28M	4.6	82.0
PGT-B (ours)	224	50M	9.1	83.4
PGT-L (ours)	224	88M	15.9	83.6

## 4.2 Semantic Image Segmentation

We evaluate the segmentation performance of our FTN on PASCAL Context [34], ADE20K dataset [61] and COCO-Stuff [4] datasets.

**Datasets.** PASCAL Context [34] is an extension of the PASCAL VOC 2010 detection challenge. Due to the sparsity of some categories, a subset of 60 classes is more commonly used. For fair comparisons, we also use this 60 classes (59 classes and background) subset, which contains 4998 and 5105 images for training and validation, respectively. ADE20K [61] is a more challenging scene parsing dataset, which is split into 20210, 2000 and 3352 images for training, validation and testing, respectively, with 150 fine-grained object categories. COCO-Stuff-10K [4] has 9000 training images and 1000 testing images with 182 categories, which is referred as COCO-Stuff in this paper.

**Experimental Details.** We optimize our models using AdamW [31] with a batch size of 16. The total iterations are set to 80k, 160k and 100k for PASCAL Context, ADE20K and COCO-Stuff respectively. The initial learning rate is set to  $2e-5$  with polynomial decay scheduler and weight decay 0. During training, data augmentation in all the experiments consists of three steps: (i) random horizontal flipping, (ii) random scale with factors between 0.5 and 2, (iii) random cropping 480 for PASCAL Context and 512 for ADE20K and COCO-Stuff. During inference, the multi-scale (MS) (factors vary from 0.5 to 1.75 with 0.25 as interval) mIoU is reported. For a fair comparison, we simply apply the cross-entropy loss and synchronized BN. Auxiliary losses are added to the output of each FPT branch with a weight of 0.1, which is slightly beneficial to the precise prediction.

**Results on PASCAL Context.** Table 3 shows the results on PASCAL Context dataset. Our FTN with PGT variants as encoder are significantly superior to the corresponding UperNet(Swin) models with similar numbers of parameters and computation cost. For example, our FTN(PGT-S) is +4.1% higher than UperNet(Swin-T) (53.09 vs.48.99). Our FTN(PGT-L) achieves 56.05% mIoU, outperforming the UperNet(Swin-B) with 52.57% mIoU by a large margin. Surprisingly, our FTN (PGT-L) which pretrained on ImageNet-1K surpasses the SETR-MLA(ViT-L/16) by +0.22%,

Table 3: Comparisons with the state-of-the-art segmentation models on PASCAL Context, ADE20K and COCO-Stuff datasets. All the mIoU is obtained by multi-scale inference. “\*” denotes our implementation using the official code. “‡” indicates pretraining on larger ImageNet-21k dataset under the input size of  $384 \times 384$ . “-” means no public results available.

Method	Encoder		mIoU		
	Model	Params	PASCAL Context	ADE20K	COCO-Stuff
FCN [30]	ResNet-101 [19]	45M	45.63	41.40	-
PSPNet [59]	ResNet-101 [19]	45M	47.78	45.35	-
DeepLabV3+ [8]	ResNet-101 [19]	45M	48.47	46.35	-
DANet [15]	ResNet-101 [19]	45M	52.60	45.02	39.70
OCRNet [54]	ResNet-101 [19]	45M	54.80	45.28	39.50
GINet [49]	ResNet-101 [19]	45M	54.90	45.54	40.60
Efficient-FCN[28]	ResNet-101 [19]	45M	53.30	45.28	-
RecoNet [9]	ResNet-101 [19]	45M	54.80	45.54	41.50
UperNet [50]	Swin-T [29]	28M	48.99*	45.81	39.13*
UperNet [50]	Swin-S [29]	50M	51.66*	49.47	41.58*
UperNet [50]	Swin-B [29]	88M	52.57*	49.72	42.20*
UperNet [50]	Swin-L ‡ [29]	197M	57.29*	53.50	47.71*
SETR-MLA [60]	ViT-L/16 ‡ [13]	307M	55.83	50.28	-
FTN (ours)	PGT-T	13M	51.15	45.17	41.57
FTN (ours)	PGT-S	28M	53.09	47.50	43.63
FTN (ours)	PGT-B	50M	54.93	50.02	44.82
FTN (ours)	PGT-L	88M	56.05	50.19	45.89
FTN (ours)	Swin-L ‡ [29]	197M	58.52	53.64	48.48

whose encoder pretrained on a larger ImageNet-21K dataset. Furthermore, with a stronger backbone Swin-L, FTN achieves the new state-of-the-art 58.52% mIoU, +2.69% and +1.23% higher than SETR-MLA(ViT-L/16) and UperNet(Swin-L), respectively.

**Results on ADE20K.** As shown in Table 3, we compare the performance of FTN with the famous and state-of-the-art models on the more challenging ADE20K validation dataset. Compared with CNN-based models, our FTN has achieved overwhelming advantages with even a lower complexity, such as (47.50% vs. 46.35%). Besides, our FTN(PGT) models still outperform UperNet(Swin) under similar computational burden by about +0.5% mIoU. When using the Swin-L which is pretrained on larger dataset as encoder, our FTN(Swin-L) achieves 53.64% mIoU, and is +0.14% higher than the previous best UperNet(Swin-L) with 53.50% mIoU.

**Results on COCO-Stuff.** The state-of-the-art results on COCO-Stuff dataset are shown in Table 3. RecoNet with ResNet-101 as the backbone achieves a mIoU of 41.50%, which is the most advanced CNN model. Our FTN(PGT-T) is comparable to the most advanced CNN model (41.57 vs. 41.50) with three times reduction in the numbers of parameters. Our FTN(PGT) models are significantly superior to the promising Swin Transformers, with the advantages of about 4%. Our FTN(Swin-L) finally achieves 48.48% mIoU, which is +0.77% higher than the state-of-the-art UperNet(Swin-L) by a large margin.

### 4.3 Ablation Study

In this section, we first replace the encoder and decoder of our FTN with other models for comparisons to demonstrate the effectiveness of PGT and FPT, respectively. Then, we conduct the ablation study about the group choices of our PGT.

**Effectiveness of PGT.** Our proposed FTN is a general and flexible fully transformer framework for image segmentation, in which the encoder can be replaced by any other transformer backbones. In order to prove the effectiveness of PGT, we compare the recent promising transformer backbones, such as ViT [13], PVT [46] and Swin Transformer [29] with our PGT under various decoders on PASCAL Context. As shown in Table 4, no matter which decoder is used, our PGT variants are about +3~6% higher than PVTs and +2~4% higher than Swins on average with similar computation burdens, which demonstrate the superiority of our PGT for segmentation. It is remarkable that our

Table 4: Combinations of different encoders and decoders on PASCAL Context validation dataset. ‡ refers to pretraining on a larger ImageNet-21k dataset under the input size of  $384 \times 384$ . For a fair comparison, all the settings are same as mentioned in Section 4.2, except that the auxiliary layers are removed and the total iteration is halved to 40k.

Encoder		Decoder						
Model	Params	CNN				Transformer		
		Semantic FPN [23]	SETR-PUP [60]	SETR-MLA [60]	DPT [38]	UperNet [50]	Trans2Seg [51]	FPT(ours)
PVT-Tiny [46]	13M	43.34	41.13	43.50	43.67	43.92	43.03	44.62
PGT-T (ours)	13M	49.04	46.59	49.21	48.63	49.95	49.56	50.48
PVT-Small [46]	25M	47.53	45.44	47.63	47.13	47.95	46.19	48.43
Swin-T [29]	28M	47.01	44.43	47.29	47.25	48.95	47.42	49.42
PGT-S (ours)	28M	50.37	47.94	50.91	50.67	51.58	50.83	51.93
Swin-S [29]	50M	50.03	47.10	50.77	50.51	51.76	50.17	52.43
PVT-Large [46]	61M	49.70	47.20	50.27	49.52	50.53	49.72	51.08
PGT-B (ours)	50M	53.26	50.29	53.73	53.24	54.02	53.44	54.06
Swin-B [29]	88M	50.31	47.52	51.18	52.17	52.51	50.80	53.35
ViT-L/16 ‡ [13]	307M	52.65	52.42	52.87	52.65	52.93	52.78	53.43
PGT-L (ours)	88M	54.09	52.61	54.60	54.31	54.73	54.13	55.24

PGT-L even surpasses the more computationally intensive ViT-Large (pretrained on ImageNet-21K) by +1~2% improvement with considerably fewer amount of pretraining data.

**Effectiveness of FPT.** Meanwhile, the decoder part of FTN is also compatible with various CNN and transformer-based decoders. To evaluate the effectiveness of our FPT, we compare FPT with the decoders used in previous transformer segmentation models on PASCAL Context dataset. Experiments in Table 4 show that no matter which backbone is applied, our FPT is consistently superior to other popular decoders, about +1% higher than Semantic FPN and about +0.5% higher than UperNet used in [29]. Compared with another query-based transformer decoder proposed in Trans2Seg [51], our FPT also performs better by a large margin (55.24 vs. 54.13).

**Group Choices of PGT.** As mentioned in Section 3.2, receptive fields of PGT can be adjusted by the group numbers of encoder stages. Excessive receptive fields will impose a heavy computational burden, while if the receptive field is too small, it will be insufficient for context modeling. Figure 4 shows the comparison with different choices of PGT group numbers in four encoder stages. PGT<64-16-1-1> is +0.38% better than PGT<64-16-4-1> with fewer additional computation, which demonstrates that global context modeling on the 1/16 resolution features in stage 3 is critical to the performance. PGT<16-4-1-1> is slightly +0.02% better than PGT<64-16-1-1>, but much more expensive for memory cost. As a result, we use PGT<64-16-1-1> in our PGT variants.

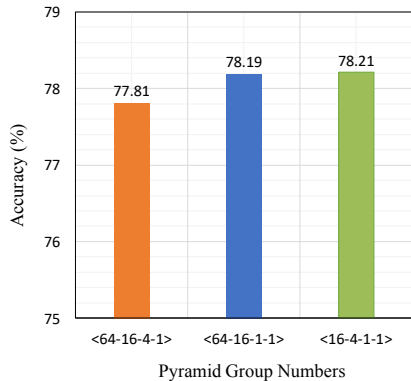


Figure 4: Different receptive fields of PGT. The a, b, c, d in <a-b-c-d> represent the group number in stage 1~4 respectively.

## 5 Conclusion

We have developed the Fully Transformer Networks (FTN) for semantic image segmentation. The core contributions of FTN are the proposed Pyramid Group Transformer (PGT) encoder and Feature Pyramid Transformer (FPT) decoder. The former learns hierarchical representations, which creates Pyramid Group Multi-head Self Attention to dramatically improve the efficiency and reduce the computation costs of the traditional Multi-head Self Attention. The latter fuses semantic-level and spatial-level information from multiple stages of the encoder, which can promote to the generation of finer segmentation results. Extensive experimental results on PASCAL-Context, ADE20K and COCO-Stuff have shown that our FTN can outperform the state-of-the-art methods in semantic image segmentation, demonstrating that the Fully Transformer Networks can achieve better results than hybrid transformer and CNN approaches.

## References

- [1] Ba, J.L., Kiros, J.R., Hinton, G.E.: Layer normalization. arXiv preprint arXiv:1607.06450 (2016)
- [2] Badrinarayanan, V., Kendall, A., Cipolla, R.: Segnet: A deep convolutional encoder-decoder architecture for image segmentation. *IEEE transactions on pattern analysis and machine intelligence* **39**(12), 2481–2495 (2017)
- [3] Bello, I., Zoph, B., Vaswani, A., Shlens, J., Le, Q.V.: Attention augmented convolutional networks. In: *Proceedings of the IEEE/CVF International Conference on Computer Vision*. pp. 3286–3295 (2019)
- [4] Caesar, H., Uijlings, J., Ferrari, V.: Coco-stuff: Thing and stuff classes in context. In: *Proceedings of the IEEE conference on computer vision and pattern recognition*. pp. 1209–1218 (2018)
- [5] Carion, N., Massa, F., Synnaeve, G., Usunier, N., Kirillov, A., Zagoruyko, S.: End-to-end object detection with transformers. In: *European Conference on Computer Vision*. pp. 213–229. Springer (2020)
- [6] Chen, L.C., Papandreou, G., Kokkinos, I., Murphy, K., Yuille, A.L.: Deeplab: Semantic image segmentation with deep convolutional nets, atrous convolution, and fully connected crfs. *IEEE transactions on pattern analysis and machine intelligence* **40**(4), 834–848 (2017)
- [7] Chen, L.C., Papandreou, G., Schroff, F., Adam, H.: Rethinking atrous convolution for semantic image segmentation. arXiv preprint arXiv:1706.05587 (2017)
- [8] Chen, L.C., Zhu, Y., Papandreou, G., Schroff, F., Adam, H.: Encoder-decoder with atrous separable convolution for semantic image segmentation. In: *Proceedings of the European conference on computer vision (ECCV)*. pp. 801–818 (2018)
- [9] Chen, W., Zhu, X., Sun, R., He, J., Li, R., Shen, X., Yu, B.: Tensor low-rank reconstruction for semantic segmentation. In: *European Conference on Computer Vision*. pp. 52–69. Springer (2020)
- [10] Chu, X., Tian, Z., Zhang, B., Wang, X., Wei, X., Xia, H., Shen, C.: Conditional positional encodings for vision transformers. arXiv preprint arXiv:2102.10882 (2021)
- [11] Cordts, M., Omran, M., Ramos, S., Rehfeld, T., Enzweiler, M., Benenson, R., Franke, U., Roth, S., Schiele, B.: The cityscapes dataset for semantic urban scene understanding. In: *Proceedings of the IEEE conference on computer vision and pattern recognition*. pp. 3213–3223 (2016)
- [12] Cubuk, E.D., Zoph, B., Mane, D., Vasudevan, V., Le, Q.V.: Autoaugment: Learning augmentation strategies from data. In: *Proceedings of the IEEE/CVF Conference on Computer Vision and Pattern Recognition*. pp. 113–123 (2019)
- [13] Dosovitskiy, A., Beyer, L., Kolesnikov, A., Weissenborn, D., Zhai, X., Unterthiner, T., Dehghani, M., Minderer, M., Heigold, G., Gelly, S., et al.: An image is worth 16x16 words: Transformers for image recognition at scale. arXiv preprint arXiv:2010.11929 (2020)
- [14] Fan, H., Xiong, B., Mangalam, K., Li, Y., Yan, Z., Malik, J., Feichtenhofer, C.: Multiscale vision transformers. arXiv preprint arXiv:2104.11227 (2021)
- [15] Fu, J., Liu, J., Tian, H., Li, Y., Bao, Y., Fang, Z., Lu, H.: Dual attention network for scene segmentation. In: *Proceedings of the IEEE/CVF Conference on Computer Vision and Pattern Recognition*. pp. 3146–3154 (2019)
- [16] Gupta, J., Saini, S.K., Juneja, M.: Survey of denoising and segmentation techniques for mri images of prostate for improving diagnostic tools in medical applications. *Materials Today: Proceedings* **28**, 1667–1672 (2020)
- [17] Han, K., Xiao, A., Wu, E., Guo, J., Xu, C., Wang, Y.: Transformer in transformer. arXiv preprint arXiv:2103.00112 (2021)
- [18] Harders, M., Szekely, G.: Enhancing human-computer interaction in medical segmentation. *Proceedings of the IEEE* **91**(9), 1430–1442 (2003)
- [19] He, K., Zhang, X., Ren, S., Sun, J.: Deep residual learning for image recognition. In: *Proceedings of the IEEE conference on computer vision and pattern recognition*. pp. 770–778 (2016)

- [20] Howard, J., Ruder, S.: Universal language model fine-tuning for text classification. arXiv preprint arXiv:1801.06146 (2018)
- [21] Huang, G., Sun, Y., Liu, Z., Sedra, D., Weinberger, K.Q.: Deep networks with stochastic depth. In: European conference on computer vision. pp. 646–661. Springer (2016)
- [22] Huang, Z., Wang, X., Huang, L., Huang, C., Wei, Y., Liu, W.: Ccnet: Criss-cross attention for semantic segmentation. In: Proceedings of the IEEE/CVF International Conference on Computer Vision. pp. 603–612 (2019)
- [23] Kirillov, A., Girshick, R., He, K., Dollár, P.: Panoptic feature pyramid networks. In: Proceedings of the IEEE/CVF Conference on Computer Vision and Pattern Recognition. pp. 6399–6408 (2019)
- [24] Krähenbühl, P., Koltun, V.: Efficient inference in fully connected crfs with gaussian edge potentials. *Advances in neural information processing systems* **24**, 109–117 (2011)
- [25] Lee, C.H., Liu, Z., Wu, L., Luo, P.: Maskgan: Towards diverse and interactive facial image manipulation. In: Proceedings of the IEEE/CVF Conference on Computer Vision and Pattern Recognition. pp. 5549–5558 (2020)
- [26] Li, Y., Zhang, K., Cao, J., Timofte, R., Van Gool, L.: Localvit: Bringing locality to vision transformers. arXiv preprint arXiv:2104.05707 (2021)
- [27] Lin, T.Y., Dollár, P., Girshick, R., He, K., Hariharan, B., Belongie, S.: Feature pyramid networks for object detection. In: Proceedings of the IEEE conference on computer vision and pattern recognition. pp. 2117–2125 (2017)
- [28] Liu, J., He, J., Zhang, J., Ren, J.S., Li, H.: Efficientfcn: Holistically-guided decoding for semantic segmentation. In: European Conference on Computer Vision. pp. 1–17. Springer (2020)
- [29] Liu, Z., Lin, Y., Cao, Y., Hu, H., Wei, Y., Zhang, Z., Lin, S., Guo, B.: Swin transformer: Hierarchical vision transformer using shifted windows. arXiv preprint arXiv:2103.14030 (2021)
- [30] Long, J., Shelhamer, E., Darrell, T.: Fully convolutional networks for semantic segmentation. In: Proceedings of the IEEE conference on computer vision and pattern recognition. pp. 3431–3440 (2015)
- [31] Loshchilov, I., Hutter, F.: Decoupled weight decay regularization. arXiv preprint arXiv:1711.05101 (2017)
- [32] Luo, W., Li, Y., Urtasun, R., Zemel, R.: Understanding the effective receptive field in deep convolutional neural networks. arXiv preprint arXiv:1701.04128 (2017)
- [33] McCann, B., Bradbury, J., Xiong, C., Socher, R.: Learned in translation: Contextualized word vectors. arXiv preprint arXiv:1708.00107 (2017)
- [34] Mottaghi, R., Chen, X., Liu, X., Cho, N.G., Lee, S.W., Fidler, S., Urtasun, R., Yuille, A.: The role of context for object detection and semantic segmentation in the wild. In: Proceedings of the IEEE Conference on Computer Vision and Pattern Recognition. pp. 891–898 (2014)
- [35] Noh, H., Hong, S., Han, B.: Learning deconvolution network for semantic segmentation. In: Proceedings of the IEEE international conference on computer vision. pp. 1520–1528 (2015)
- [36] Polyak, B.T., Juditsky, A.B.: Acceleration of stochastic approximation by averaging. *SIAM journal on control and optimization* **30**(4), 838–855 (1992)
- [37] Radosavovic, I., Kosaraju, R.P., Girshick, R., He, K., Dollár, P.: Designing network design spaces. In: Proceedings of the IEEE/CVF Conference on Computer Vision and Pattern Recognition. pp. 10428–10436 (2020)
- [38] Ranftl, R., Bochkovskiy, A., Koltun, V.: Vision transformers for dense prediction. arXiv preprint arXiv:2103.13413 (2021)
- [39] Russakovsky, O., Deng, J., Su, H., Krause, J., Satheesh, S., Ma, S., Huang, Z., Karpathy, A., Khosla, A., Bernstein, M., et al.: Imagenet large scale visual recognition challenge. *International journal of computer vision* **115**(3), 211–252 (2015)
- [40] Szegedy, C., Liu, W., Jia, Y., Sermanet, P., Reed, S., Anguelov, D., Erhan, D., Vanhoucke, V., Rabinovich, A.: Going deeper with convolutions. In: Proceedings of the IEEE conference on computer vision and pattern recognition. pp. 1–9 (2015)

- [41] Szegedy, C., Vanhoucke, V., Ioffe, S., Shlens, J., Wojna, Z.: Rethinking the inception architecture for computer vision. In: Proceedings of the IEEE conference on computer vision and pattern recognition. pp. 2818–2826 (2016)
- [42] Te, G., Liu, Y., Hu, W., Shi, H., Mei, T.: Edge-aware graph representation learning and reasoning for face parsing. In: European Conference on Computer Vision. pp. 258–274. Springer (2020)
- [43] Teichmann, M.T., Cipolla, R.: Convolutional crfs for semantic segmentation. arXiv preprint arXiv:1805.04777 (2018)
- [44] Touvron, H., Cord, M., Douze, M., Massa, F., Sablayrolles, A., Jégou, H.: Training data-efficient image transformers & distillation through attention. arXiv preprint arXiv:2012.12877 (2020)
- [45] Vaswani, A., Shazeer, N., Parmar, N., Uszkoreit, J., Jones, L., Gomez, A.N., Kaiser, L., Polosukhin, I.: Attention is all you need. arXiv preprint arXiv:1706.03762 (2017)
- [46] Wang, W., Xie, E., Li, X., Fan, D.P., Song, K., Liang, D., Lu, T., Luo, P., Shao, L.: Pyramid vision transformer: A versatile backbone for dense prediction without convolutions. arXiv preprint arXiv:2102.12122 (2021)
- [47] Wang, X., Girshick, R., Gupta, A., He, K.: Non-local neural networks. In: Proceedings of the IEEE conference on computer vision and pattern recognition. pp. 7794–7803 (2018)
- [48] Wu, H., Xiao, B., Codella, N., Liu, M., Dai, X., Yuan, L., Zhang, L.: Cvt: Introducing convolutions to vision transformers. arXiv preprint arXiv:2103.15808 (2021)
- [49] Wu, T., Lu, Y., Zhu, Y., Zhang, C., Wu, M., Ma, Z., Guo, G.: Ginet: Graph interaction network for scene parsing. In: European Conference on Computer Vision. pp. 34–51. Springer (2020)
- [50] Xiao, T., Liu, Y., Zhou, B., Jiang, Y., Sun, J.: Unified perceptual parsing for scene understanding. In: Proceedings of the European Conference on Computer Vision (ECCV). pp. 418–434 (2018)
- [51] Xie, E., Wang, W., Wang, W., Sun, P., Xu, H., Liang, D., Luo, P.: Segmenting transparent object in the wild with transformer. arXiv preprint arXiv:2101.08461 (2021)
- [52] Xie, S., Girshick, R., Dollár, P., Tu, Z., He, K.: Aggregated residual transformations for deep neural networks. In: Proceedings of the IEEE conference on computer vision and pattern recognition. pp. 1492–1500 (2017)
- [53] Yuan, L., Chen, Y., Wang, T., Yu, W., Shi, Y., Jiang, Z., Tay, F.E., Feng, J., Yan, S.: Tokens-to-token vit: Training vision transformers from scratch on imagenet. arXiv preprint arXiv:2101.11986 (2021)
- [54] Yuan, Y., Chen, X., Wang, J.: Object-contextual representations for semantic segmentation. arXiv preprint arXiv:1909.11065 (2019)
- [55] Zeiler, M.D., Fergus, R.: Visualizing and understanding convolutional networks. In: European conference on computer vision. pp. 818–833. Springer (2014)
- [56] Zhang, H., Cisse, M., Dauphin, Y.N., Lopez-Paz, D.: mixup: Beyond empirical risk minimization. arXiv preprint arXiv:1710.09412 (2017)
- [57] Zhang, P., Dai, X., Yang, J., Xiao, B., Yuan, L., Zhang, L., Gao, J.: Multi-scale vision longformer: A new vision transformer for high-resolution image encoding. arXiv preprint arXiv:2103.15358 (2021)
- [58] Zhang, Q.s., Zhu, S.C.: Visual interpretability for deep learning: a survey. *Frontiers of Information Technology & Electronic Engineering* **19**(1), 27–39 (2018)
- [59] Zhao, H., Shi, J., Qi, X., Wang, X., Jia, J.: Pyramid scene parsing network. In: Proceedings of the IEEE conference on computer vision and pattern recognition. pp. 2881–2890 (2017)
- [60] Zheng, S., Lu, J., Zhao, H., Zhu, X., Luo, Z., Wang, Y., Fu, Y., Feng, J., Xiang, T., Torr, P.H., et al.: Rethinking semantic segmentation from a sequence-to-sequence perspective with transformers. arXiv preprint arXiv:2012.15840 (2020)
- [61] Zhou, B., Zhao, H., Puig, X., Xiao, T., Fidler, S., Barriuso, A., Torralba, A.: Semantic understanding of scenes through the ade20k dataset. *International Journal of Computer Vision* **127**(3), 302–321 (2019)
- [62] Zhu, Z., Xu, M., Bai, S., Huang, T., Bai, X.: Asymmetric non-local neural networks for semantic segmentation. In: Proceedings of the IEEE/CVF International Conference on Computer Vision. pp. 593–602 (2019)

## Appendix

In this appendix, we first provide more ablation experiments on ImageNet [39] and COCO-Stuff [4] to evaluate some appropriate design choices of Pyramid Group Transformer (PGT) and Feature Pyramid Transformer (FPT), respectively. Then, we show some visualization results on PASCAL-Context [34], ADE20K [61] and COCO-Stuff [4]. Finally, we evaluate the generalization of our Fully Transformer Networks (FTN) on other dense prediction tasks.

### A Ablation study for PGT

#### A.1 Position Encoding Methods

Positional embeddings are used to introduce the awareness of spatial location for self-attention, which have been proved to be critical to Transformers [45, 13, 29, 10]. To understand the effect of position encoding methods for our PGT, we compare four different settings, namely no position encoding (*no pos.*), learnable absolute position encoding (*LE*)[13], conditional position encoding (*CPE*)[10] and a combination of *LE* and *CPE* (*LE&CPE*). As shown in Figure 5, *LE* achieves +1.16% higher than *no pos.*, which shows the importance of position encoding. *CPE* achieves +0.7% higher than *LE* and +0.34% higher than *LE&CPE*. Furthermore, *CPE* is compatible with variable-length input sequences, which is an obvious limitation of absolute position encoding. Therefore, we use *CPE* in our PGT as an implicit position encoding scheme.

#### A.2 CLS-Token

CLS-Token plays the role of a global image representation, which is expected to contain all of discriminate information for final classification. Some of Vision Transformers kept CLS-Token throughout the network[13], while some works only involved it at the last stage[46]. Considering that CLS-Token may have missed some key information, [29] directly removed the CLS-Token and applied average pooling on the last output of the backbone instead. Inspired by above all, we study the impact of four CLS-token patterns for PGT. As shown in Figure 6, average pooling performs the best, achieving +0.37% and +0.48% higher than the CLS-token in only stage4 and all stages respectively. Thus, in PGT, we simply apply average pooling on the final output of stage 4 to generate a global token rather than CLS-Token.

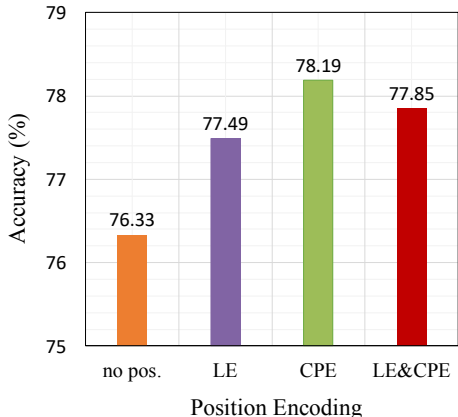


Figure 5: Different position encoding approaches in PGT.

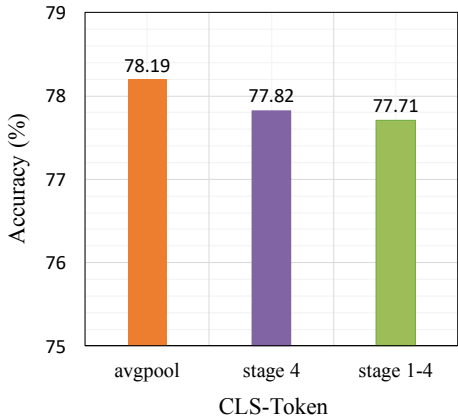


Figure 6: Different CLS-Token in PGT.

Table 5: Comparisons of different settings of FPT. <a-b-c> represents the settings for the transformer blocks which are performed on the feature maps with stride 32("a"), 16("b") and 8("c"), respectively. The mIoU is obtained by multi-scale inference on COCO-Stuff validation dataset.

Depth	Embedding dim	SR-MSA ratio	Fusion mode	mIoU (%)
<1-1-1>	256	<2-2-2>	add	42.41
<1-1-1>	512	<2-2-2>	add	43.37
<1-2-1>	512	<2-2-2>	add	43.11
<1-1-1>	512	<1-2-2>	add	43.26
<1-1-1>	512	<1-1-2>	add	43.33
<1-1-1>	512	<2-2-2>	concat	43.35

## B Ablation study for FPT

### B.1 Scales of FPT

With the limited segmentation training data, the scale of decoder is not the larger the better for segmentation [51], so that there is an important trade-off between the scale of FPT and the performance. In our FPT, the scale is mainly determined by depth, embedding dim, and the reduction ratio of SR-MSA. In this section, we compare different combinations of these hyper-parameters with PGT-S as the backbone on COCO-Stuff validation set. All the settings are the same as Section 4.2, except the abandoned auxiliary layers.

**Depth.** Considering that features with stride 16 have a good trade-off in terms of containing semantic and detailed information, we try to enlarge the depth (number of blocks) for transformer blocks with 1/16 features in FPT. As shown in Table 5, increasing the depth for 1/16 features results in a 0.26% mIoU drop (43.37 vs. 43.11), which indicates that the FPT decoder is not the deeper the better.

**Embedding dim.** Embedding dim refers to the dimension of tokens in transformer blocks of FPT. Excessive small embedding dim might lead to the lack of representation ability, and a too large one may result in channel redundancy and increased computational burden. Considering the constraints of computing resources, we tried two computation-friendly choices of embedding dims ( $dim=256$  and  $512$ ). As shown in Table 5,  $dim=512$  is significantly superior to  $dim=256$  (43.37 vs. 42.41). Therefore, we set the embedding dim to 512 in our FPT.

**Reduction ratio of SR-MSA.** In our FPT, SR-MSA is used to reduce memory and computation cost by spatially reducing the number of key and value tokens, especially for high-resolution representations. Considering that the token numbers of the low-resolution features are relatively fewer, we attempt to remove the spatial reduction for transformer blocks with 1/32 and 1/16 features. Table 5 compares the different choices of reduction ratio of SR-MSA in FPT. It turns out that without using SR-MSA on low-resolution representations, the computation cost is increased, while there is no significant performance gain as expected (43.37 vs. 43.33 vs. 43.26). On the contrary, not using SR-MSA results in slight performance degradation.

### B.2 Fusion mode of FPT

In our FPT, the multi-level high-resolution features of each branch need to be fused to generate finer prediction. We explore two simple fusion mode, *i.e.*, element-wise summation and channel-wise concatenation. As shown in Table 5, summation performs +0.02% slightly better than concatenation, thus we fuse the multi-level representations by the simpler and more efficient element-wise summation.

## C Visualization

In this section, we illustrate the visualization results on the three benchmarks, such as PASCAL Context (Figure 7), ADE20K (Figure 8) and COCO-Stuff (Figure 9), respectively. We mainly compare our FTN with UperNet [50], which is the current state-of-the-art method. According to these segmentation results, we can see that our FTN(Swin-L) performs better in distinguishing the confusing regions with similar colors but different categories. For example, in Line 4 of Figure 7,

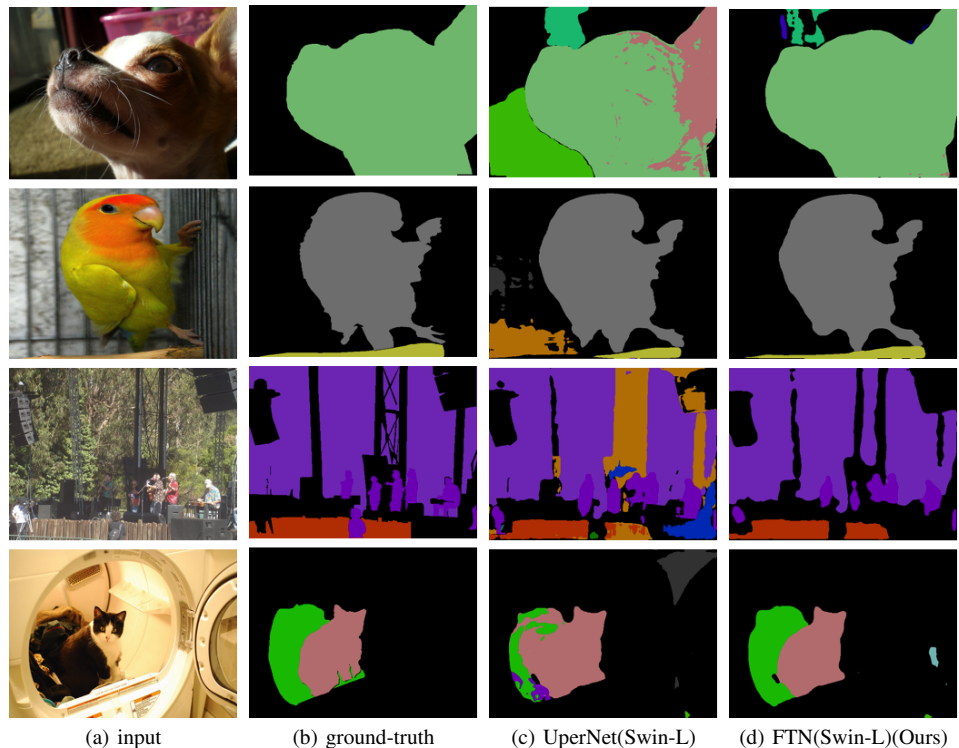


Figure 7: Visualization comparison on PASCAL Context dataset.

Table 6: Comparisons with state-of-the-arts on CelebAMask-HQ validation dataset. The commonly-used mean F1-score (over all the foreground categories) is used for evaluation.

Method	mean F1
PSPNet [59]	76.2
MaskGAN [25]	80.3
EAGRNet [42]	85.1
UperNet(Swin-L) [29]	85.5
FTN(Swin-L) (ours)	85.9

UperNet(Swin-L) confused the cat with its surrounding clothing, while our FTN(Swin-L) distinguish them clearly. However, UperNet(Swin-L) will confuse in some visually easy areas. For example, in the second and third row of Figure 3, the bird and its background are visually distinct, which is visually a simple scene, while UperNet(Swin-L) misjudges some part of the background surprisingly.

## D Results on Face Parsing

In order to evaluate the generalization of our FTN on other dense prediction tasks, we also apply our FTN(Swin-L) on the face parsing task, which aims to distinguish between different parts of the face, such as eyes, nose, and mouth. We compare our model with the state-of-the-arts on CelebAMask-HQ dataset [25]. CelebAMask-HQ is a large-scale face parsing dataset with 19 categories including some additional eyeglass, earring, necklace, neck, and cloth beyond the traditional facial components. It contains 24183, 2993, and 2824 images for training, validation, and testing respectively. As shown in Table 6, our FTN(Swin-L) surpasses the best transformer-based method UperNet(Swin-L) with +0.4%. Compared with previous CNN-based models, our FTN(Swin-L) also outperforms them by a large margin (85.9 vs. 85.1). Figure 10 presents the visualization comparisons, which shows that the segmentation of our FTN(Swin-L) is more detailed.

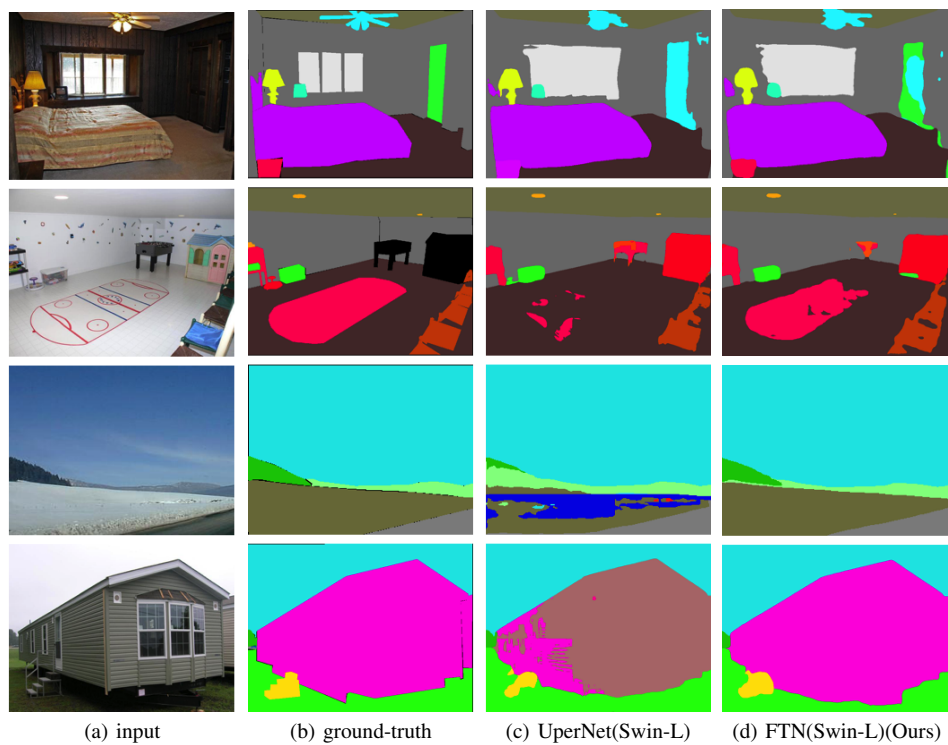


Figure 8: Visualization comparison on ADE20K dataset.



Figure 9: Visualization comparison on COCO-Stuff dataset.

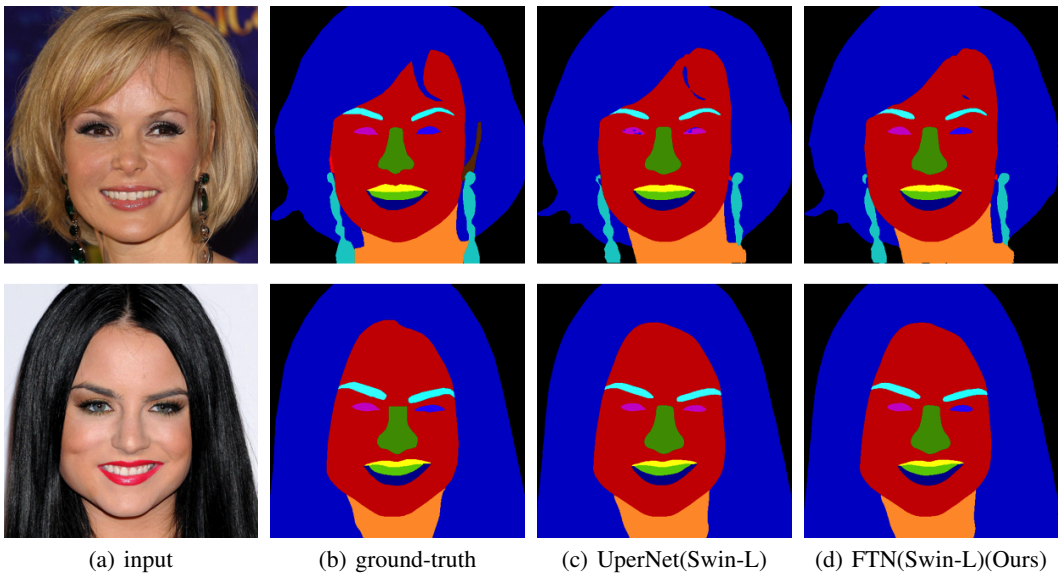


Figure 10: Visualization comparison on CelebAMask-HQ dataset.